Surf zone bubble populations

E. J. Terrill, G. Lada, W. K. Melville
Scripps Institution of Oceanography, mail code 0213, La Jolla, CA 92093-0213, USA.
et@mpl.ucsd.edu, grlada@mpl.ucsd.edu, kmelville@mpl.ucsd.edu

Abstract

Breaking waves in the surf zone entrain high-density bubble clouds which can be transported some distance offshore the region of active breaking via rip currents and turbulent mixing processes. Understanding the physical processes which govern the nearshore bubble populations is paramount to understanding high-frequency sound propagation in the littoral region. A combined measurement and modeling effort designed to improve our understanding of the populations transported by rip currents, and their impact on sound propagation, is presented.

1. Introduction

The presence of bubbles in the littoral region introduces complexity in understanding the propagation of natural and man-made sound in this region. Nearshore bubble populations are also studied for their ability to enhance atmospheric gas exchange, generate marine aerosols, and change the remote-sensing reflectance of coastal waters. After bubbles are injected into the water column, their lifetimes are governed by their rise velocity, turbulent mixing, and gas dissolution, while their distribution in space depends largely on currents. As a result, the study of the generation and lifetimes of oceanic bubble populations is a complex field which spans multiple scientific disciplines. Both measurement and physical modeling efforts are necessary to provide insight into the generation and lifetimes of oceanic bubble populations. These two aspects of bubble research are described in the context of bubbles generated in the surf and their offshore transport by rip currents.

2. Field Measurements

A field experiment aimed at characterizing the nearshore bubble size distributions, and measure their effects on underwater sound propagation, was performed March 1-12, 1997 near the Scripps Pier in La Jolla, California. The multi-investigator experiment had participants from the U.S. Naval Research Laboratory, the Institute of Ocean Sciences, the Applied Physics Laboratory (University of Washington), and the National Center for Physical Acoustics. As part of our efforts in the field campaign, we deployed a vertical array of broadband acoustic modules O(100) m offshore the surf zone in a water depth which ranged between 6-8 m depending on the phase of the tide. The modules are composed of source and receive transducers spaced O(0.1) m apart. Between these a broadband acoustic pulse is transmitted, and the received signal is subsequently processed to determine the sound speed and attenuation changes resulting from bubbles present in the water. The attenuation data are subsequently inverted for bubble size distributions using an inversion technique based upon the principles described by Commander and McDonald [1] to deduce bubble size distributions at the 2 Hz ping rate. A complete description of the acoustic instrumentation and its performance in the laboratory and field can be found in [2]. For this deployment, the bandwidth of the system was between 4 kHz – 100 kHz which allowed us to resolve bubble sizes in the range 30-800 μm.

The broadband acoustic modules were mounted to a 6 m long aluminum spar at distances of 2 m, 3.2 m, 4.3 m, and 5.5 m from the base. The spar was mounted to a railcar wheel via a semi-compliant base which allowed some horizontal displacement to reduce loads in large waves. The array was deployed approximately 40 m north of the Scripps Pier in water of a nominal depth of 6 m using a large mobile crane parked on the end of the pier. Cables from the transmit and receive transducers were connected to two pressure cases mounted at the base of the spar. The pressure cases connected the cables from the acoustic modules to two multi-conductor waterproof cables, which were subsequently connected to the transmit and data acquisition hardware located in a small laboratory at the end of the pier. The ping rate used for the field system was 2 Hz for each individual module and was synchronized to prevent acoustic interference with the other nearby acoustic systems. The distance of the array to the breaking surf was approximately 100-180 m, depending on the tides and wave conditions present. Figure 1 shows the bathymetry of the Scripps beach measured just prior to the deployment of the equipment and the location of the array.

TG Leighton, GJ Heald, HD Griffiths, G Griffiths, (eds.), 'Acoustical Oceanography', Proc. Institute of Acoustics Vol. 23 Part 2, 2001.

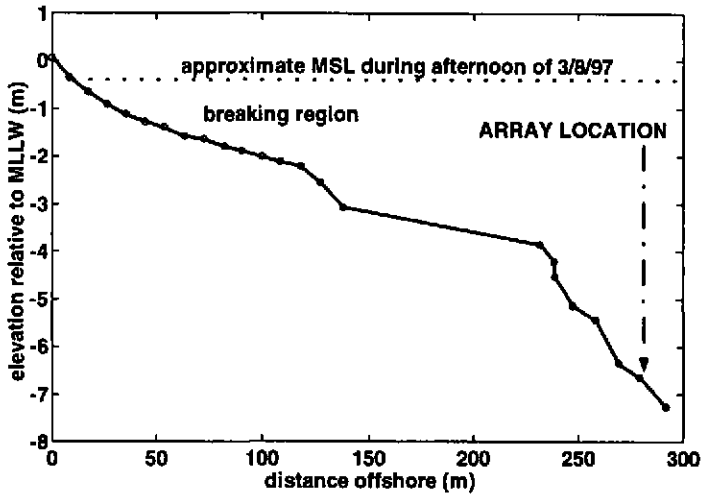

Figure 1. Bathymetry of the beach 12 m north Scripps Pier during the SIO PIER experiment.

Despite the relatively benign wind and wave conditions present during the experiment, on the afternoon of March 8, 1997, several rip currents were observed to pass through the array site. At this time, the windspeeds were less than 2 m/s and no whitecapping was present on the incoming 1 m swell. A spring low tide of –0.4 m was also present during this afternoon. As the rip currents passed through the measurement site, they intermittently advected clouds of bubbles with varying densities offshore. These bubble resulted in dramatic changes in the local acoustic properties of the offshore waters. Figure 2 presents a time series of 45 kHz attenuation measured at a depth of 1.1 m as an example of the variable nature of the bubble densities and their

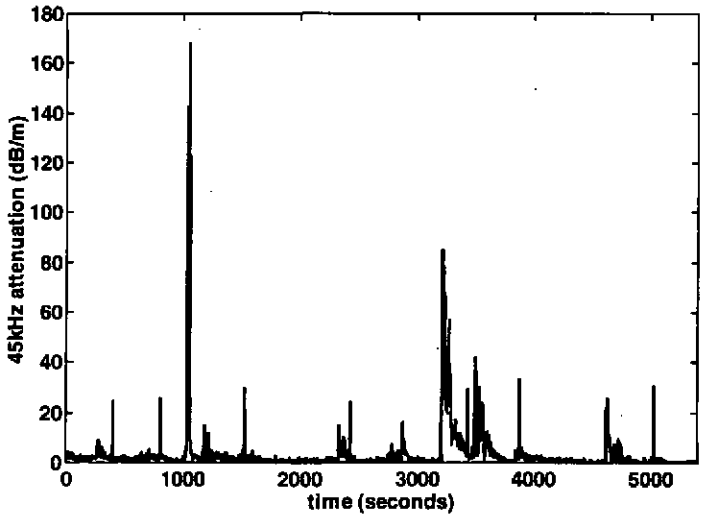

Figure 2. A 1.5 hour time series of 45 kHz attenuation measured at a depth of 1.1m offshore the surf zone.

effects on the acoustic properties. Attenuation in this frequency band was found to range from O(1) – O(100) dB/m over time periods ranging from O(5) to O(100) seconds as the collections of bubbles were transported through the measurement site. Current measurements made coincident with the acoustic events confirmed that the bubbles were only present when there were periods of offshore flow. Typical velocities of the offshore component of the rip currents were found to range from 10 cm/s to 30 cm/s – indicating that the horizontal length scales of the bubbles ranged from O(1) m to O(50) m. The velocities of the rip currents measured in the Scripps Pier Experiment are consistent with the magnitudes of rip currents reported by Smith and Largier [3] obtained with a sector-scanning Doppler sonar deployed at the end of Scripps Pier. Owing to the lack of offshore white-capping and the high coherence between the bubbles and the offshore-flow, it is concluded that the origin of the bubbles is in-shore at the region of breaking surf. The bubbles are estimated to be several minutes old based on the rip current velocities and the distance of the measurements to the breaking surf.

While the time series of attenuation at 45kHz indicates the temporal variability that results from the bubbles, it provides little indication of its frequency dependence that results from the distribution of bubble sizes within the rip current. The average attenuation present during six different rip events that are visible in Figure 2 are presented in Figure 3. The data shows a large range in peak attenuation levels ranging from a few dB/m up to 100 dB/m. The maximum attenuation was typically found between approximately 30-80 kHz, corresponding to bubbles with a resonant radius of 40-100 μm. The variations in attenuation levels and the differences in

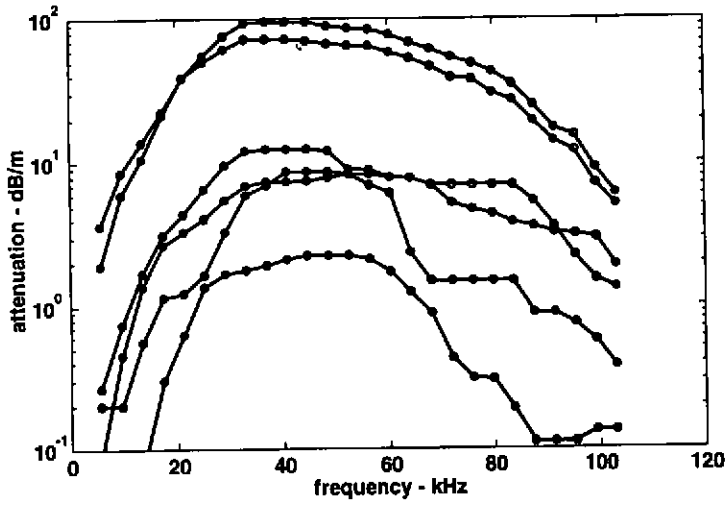

Figure 3. The frequency dependent acoustic attenuation measured during six different rip events.

the shapes of the frequency dependent attenuation indicate variability in the bubble size distributions between one event to the next. The lower frequencies appear to be more impacted during periods of denser populations.

To examine this variability in the acoustic properties, the distribution of bubble sizes within the advected bubble clouds are examined. For the 1.5 hour time series shown in Figure 2, bubble size distributions were calculated using inversions [1] based on the broadband acoustic data. The variability in the size

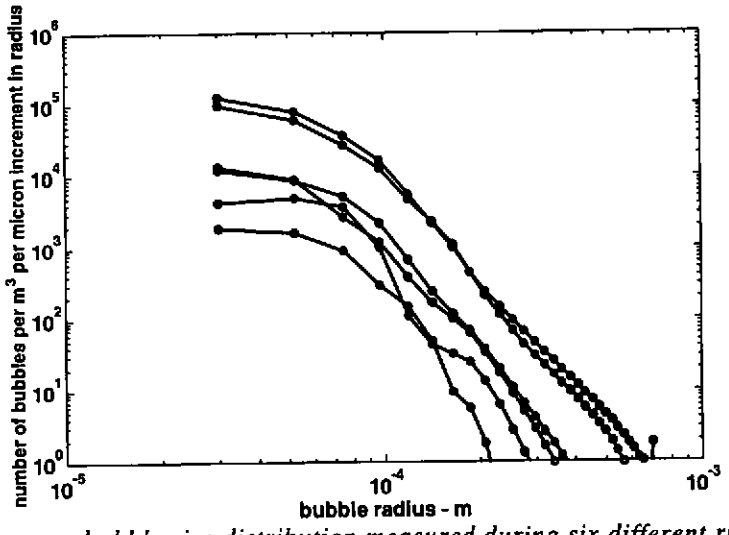

Figure 4. The average bubble size distribution measured during six different rip current events.

distributions are illustrated through examining the average bubble size distribution for the same six rip events presented above. These distributions are shown in Figure 4. The data indicates a power law behavior in the distribution at the larger radii up to some small radii cut-off ranging between 60-100 μm, followed by a flattening or roll-off of the number density at small bubble sizes. Also apparent in the data is that the power law slope is steeper for the less dense bubble populations, with power laws in the size distribution ranging from approximately a^{-8} for the least dense clouds to a^{-6} for the denser populations. This is in contrast to recent bubble size distribution measurements in much younger populations which have been found to approach an approximate power law behavior of a^{-3} in both the open ocean [4] and within surf zones [5, 6]. Clearly the physical processes

which govern the lifetimes of bubbles in the ocean impose a time-dependence on the shapes of the bubble size distribution which can be explored using physical models of the evolution of bubble populations.

3. Numerical Modelling

A simple transport model is developed to provide a physical framework for the interpretation of the bubble densities and the shapes of the bubble distributions measured during periods of rip currents. The measurements reveal that the presence of bubbles O(100) m offshore the surf zone are associated with offshore current flow. Visual observations from Scripps Pier during the experiment confirmed these episodic events with sediment and bubbles advecting offshore. It is expected that features in the bubble size distribution may be reproduced by models of turbulent transport that incorporate the governing physics which control the size distribution of the bubbles.

The equation governing a concentration of bubbles, c, of a particular radius, a, is given by:

$$\frac{\partial c}{\partial t} + u_i \frac{\partial c}{\partial x_i} = \sigma c, \tag{1}$$

where σ is a source / sink term. In a turbulent flow, the concentration and velocities can be represented as the sum of a mean and fluctuating term

$$c = \bar{c} + c', \tag{2}$$

$$u_i = \bar{u_i} + u_i'. \tag{3}$$

Substituting the above relationships into equation (1) results in

$$\frac{\partial \bar{c}}{\partial t} + \bar{u_i} \frac{\partial \bar{c}}{\partial x_i} = -\frac{\partial}{\partial x_i}(\overline{c'u_i'}) + \sigma c, \tag{4}$$

where the velocity field u_i is assumed incompressible. Representing the turbulent transport term by a second order tensor gives:

$$\overline{c'u_i'} = -K_{ij} \frac{\partial \bar{c}}{\partial x_j}, \tag{5}$$

and equation (4) can be simplified to

$$\frac{\partial \bar{c}}{\partial t} + \bar{u_i} \frac{\partial \bar{c}}{\partial x_i} = -\frac{\partial}{\partial x_i}\left[K_{ij} \frac{\partial \bar{c}}{\partial x_i}\right] + \sigma c. \tag{6}$$

Assuming the turbulence is homogenous in the fluid, K_{ij} reduces to a first order tensor, hereafter referred to as K_x, K_y, and K_z respectively.

For modeling the transport of bubbles by rip currents from the breaking surf to some distance offshore, the field is considered to be homogenous in the along-shore dimension. This allows the simplification of equation (6) to two dimensions. The familiar advection–diffusion equation that describes the environment under consideration is therefore:

$$\frac{\partial c}{\partial t} + U \frac{\partial c}{\partial x} + w_b \frac{\partial c}{\partial z} = K_x \frac{\partial^2 c}{\partial x^2} + K_z \frac{\partial^2 c}{\partial z^2} + \sigma c, \tag{7}$$

where U represents the velocity of the rip current (assumed to be uniform with depth), w_b represents the rise velocity of a bubble of radius a, and σ represents the dissolution of gas across the bubble wall. The overbar has been dropped from the mean concentration $\bar{c}$ to simplify the expression.

Equation (7) indicates that the rise-speed of the bubbles, the turbulent mixing, gas dissolution rates, and horizontal bubble advection rates are the governing physical processes which act to modify the bubble populations after their introduction through wave breaking. However it is useful to examine the relative time scales of each physical process so that their relative importance to the solution to (7) is understood. The turbulent mixing is considered first. Order of magnitude estimates of the diffusivity terms, K, can be made from reported measurements of surf zone turbulence intensity by [7]. The use of turbulent intensities measured inside the surf zone are deemed appropriate because the rip current transports both the bubbles and the turbulence generated by wave breaking. The turbulence measurements reported intensities normalized by the orbital velocities of the waves as $O(10^{-2} - 10^{-1})$ inside the surf zone. The turbulent transport coefficient can be approximated by $K \sim u'l$, where the mixing length l is assumed to be the water depth and u' is the characteristic velocity perturbations from the turbulence. Using realistic values for l, the expected range of K can be estimated to be $O(10^{-2} - 10^{-3})$ m^2s^{-1}.

As a result, the characteristic time scale for vertical mixing across the water column depth, $t_m \sim l^2/K$, is found to be $O(10^2\text{-}10^3)$ seconds for the surf zone.

Next, vertical transport due to the rise velocity of the bubbles is examined. The terminal velocity of a bubble of radius a can be calculated by considering a balance between drag forces and buoyancy forces:

$$C_D \frac{\pi a^2}{2} \rho w_b^2 = \rho g \frac{4\pi}{3} a^3 . \tag{8}$$

The drag coefficient of a bubble is typically parameterized by its Reynolds number, as suggested by Keeling [8]:

$$C_D = 24/(1+0.566\mathrm{Re}^{0.5})/\mathrm{Re}, \tag{9}$$

where the Reynolds number of the bubble is a function of its radius, rise velocity, and the kinematic viscosity of the fluid ν. This relationship in (9) was chosen as it closely agrees with both Stokes' law for surfactant-covered bubbles in the small-radius regime (a<100 μm) and overlaps the rise velocities suggested by Moore [9] for intermediate sized bubbles (100μm<a<560μm). For larger radii (a>560μm), the rise velocity is assumed to be a constant 0.30 m/s [10]. A similar functional relationship for the rise velocity has been used by Thorpe [11]. For the wide range of bubble sizes present in the surf zone, w_b will range from $O(10^{-4})$ – $O(10^{-1})$ m/s. As a result, the characteristic rise time $t_r \sim l/w_b$ of the bubble in the surf zone will range from $O(10^0\text{-}10^4)$ seconds. For example, a 100 μm bubble with a terminal velocity of approximately 1 cm/s will take 100 seconds to rise 1 m.

Last, the time scales of the dissolution of gas across the bubble wall is examined. The rate of change of a bubble radius as a result of gas flux is examined using the formulation provide by Thorpe [12]:

$$\frac{\partial a}{\partial t} = \frac{-3RT}{3pa+4\gamma}\left\{D_1 K_1 N_1\left[x\left(p+\frac{2\gamma}{a}\right)-p_{10}\right]+D_2 K_2 N_2\left[(1-x)\left(p+\frac{2\gamma}{a}\right)-p_{20}\right]\right\}, \tag{10}$$

where R is the thermal gas constant, T is the temperature, p is the hydrostatic pressure, γ is the surface tension, D is the diffusivity, K is the adsorption coefficient, and N is the Nusselt number, and p_o is the partial pressure of the dissolved gases present in the water. The subscripts one and two refer to a two component gas mixture considered to be nitrogen and oxygen in the mole fraction ratio x of 0.215. Note that as a result of variations in D, K, and N between the two gases, the mole fraction will evolve as the bubble dissolves. Simulations of (10) by Thorpe [12] indicate typical bubble decay rates 0.018 s^{-1}, resulting in a characteristic time scale of dissolution as $t_d \sim \sigma^{-1}$ equal to $O(10^1\text{-}10^2)$ seconds.

As indicated by the various time scales of the physical processes governing the lifetime of bubbles, turbulent mixing, bubble rise speed, and gas dissolution are all O(1) effects and must be included in the solution to (7). A random walk model was developed to solve (7), based on an earlier model previously developed for investigating upper ocean bubble populations [13]. Boundary conditions for the model are based on an approximation to the Scripps beach bathymetry using a constant slope of 1:50 with zero bubble flux across the bottom. The surface boundary condition allows the one way flux of bubbles across the air-sea interface; bubbles leaving the surface are lost. The initial bubble sizes introduced into the model are determined using a size distribution that varies as $n(a) \sim a^{-3}$ which is consistent with the previously mentioned bubble size distributions measured within dense clouds of bubbles [4-6] or theoretical arguments of bubble breakup based on turbulent dissipation rates [13]. The initial number density is determined by fixing the bubble sizes to range between 10-2000 μm and the void fraction set to 0.01. Bubbles are introduced inshore at a depth of 1m with a density that is constant with depth. In initializing the model, only bubble sizes from 10-200 μm are modeled since the higher rise velocity of the larger bubbles results in them rising out of solution after time scales of 30 seconds or less. At the site of bubble introduction, 2000 bubbles of each size (in 10 μm steps) are introduced in 10 cm increments from the surface to the 1 m bottom boundary. After they are introduced, they proceed through the random walk model under the various physical processes previously discussed with a time step of 1 second. The horizontal and vertical turbulent diffusivities are also assumed equal (K_x = K_z). The radius, gas mole fraction, and position of each bubble is tracked until either it dissolves completely or is lost at the sea surface. While this procedure is memory intensive owing to the large number of bubble trajectories, it prevents numerical diffusion effects which can result if the bubbles are binned according to some incremental radius while the model progresses in time. The model is run for 1500 seconds so that stable statistics are approached between the introduction of in-shore bubbles and the offshore distribution. Upon completion of the model, the bubbles are binned by 5 μm radius increments and scaled according to their initial concentration to derive size distributions as a function of space within the surf zone.

A number of model runs were conducted to examine the effects of turbulence represented by diffusivities ranging between 10^{-2} m^2s^{-1} and 10^{-3} m^2s^{-1} and for gas saturation levels ranging from 100% - 110%. The range of supersaturated conditions were chosen based on the measurements of Wallace and Wirick [14] which showed

bubble mediated O_2 super-saturation levels reaching 110% during large storm events on the Mid-Atlantic Bight. The horizontal advection speed of the bubbles by the rip current was kept fixed at 0.25m/s. Figure 5 presents modeled bubble size distributions at a 1 m depth for a range of distances offshore their introduction (10 m, 20 m, 60 m, and 100 m) for a turbulent diffusivity of 10^{-2} m^2s^{-1} and a gas saturation level of 105%. For comparison, the

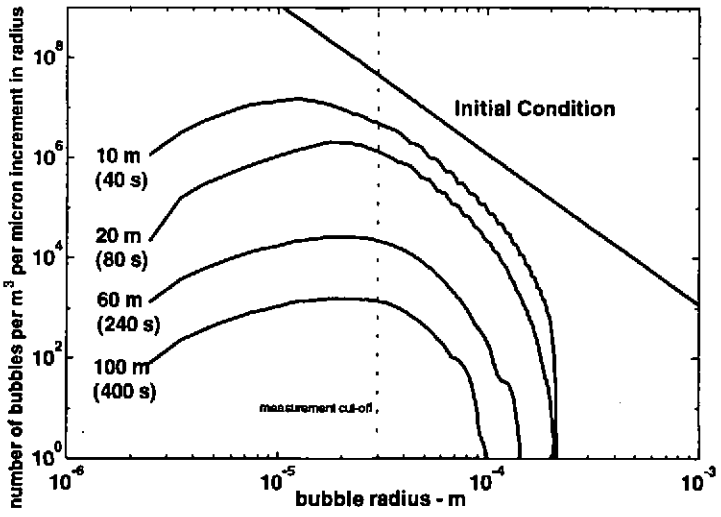

Figure 5. Bubble size distributions at various distances (times) offshore the surf zone at 1m below the water's surface for a turbulent diffusivity of 10^{-2} m^2s^{-1} and a dissolved gas saturation level of 105%. The dotted vertical line indicates the 30 μm limit of the bubble measurement equipment used in the experiment.

initial size distribution is also provided. The figure clearly demonstrates the time evolution of the bubble size distribution as it propagates offshore the surf zone. Despite the variability in rip current speeds and the uncertainty in the turbulent mixing and gas saturation levels, the model does a reasonable job of reproducing features in the measured bubble size distributions over the range of radii that the measurements extend. Both the deviation from a power law dependence and a roll off in the distribution at approximately 60 μm that is apparent in the measurements are reproduced in the model as well as the approximate number densities of the bubbles. As suggested by the model results, variability in the measured bubble size distributions could be attributed to differences in 'ages' of the bubbles that results from variability in the location of the breaking surf relative to the measurement site. These trends in the shape of the distribution as a function of distance offshore the breaking surf are consistent for model runs which varied the level of turbulent mixing or dissolved gas concentrations. The modeled bubble distributions shown in Figure 5 also exhibit a maximum in bubble densities at radii between 10-30 μm. While it is difficult to comment on the accuracy of the model at these sizes due to the 30 μm limit of the measurements, the apparent maximum in the modeled bubble densities is substantiated by recent open-ocean measurements of bubbles by Phelps and Leighton [15] who found peaks in their distributions at 18 μm.

The sensitivity of the bubble size distributions to the gas saturation levels are investigated through examination of distributions at a fixed location offshore for three model runs conducted using different gas saturation levels. The turbulent mixing terms were the same for all three runs. Figure 6 presents size distributions at a 1 m depth, 60 m offshore (approximately 240 s old bubbles) for saturation levels at 100%, 105%, and 110%. As expected, the supersaturated conditions retards the dissolution of the smaller bubble sizes (some sizes will increase in radius, depending on their depth), resulting in up to order of magnitude differences in the number density across all the bubble sizes. These results are in agreement with earlier work which examined the sensitivity of individual bubble growth rates as a function of depth and saturation level [11]. As a result of higher gas saturation levels, the smaller bubbles were found to persist much longer and subsequently were transported farther offshore. A rough estimate of this phenomena finds that the bubbles typically were transported a 100 m further offshore for each 5% increase in gas saturation level.

Last, the effects of turbulent mixing on the size distributions are examined at the same location (1 m depth, 60 m offshore) from model runs performed over a range of expected turbulent diffusivities. The response of the size distribution to the turbulent mixing is demonstrated in Figure 7. At the larger bubble sizes (approximately $a > 60\mu m$), the effect of the turbulence is an increase in more larger bubbles while the opposite is true at the smaller

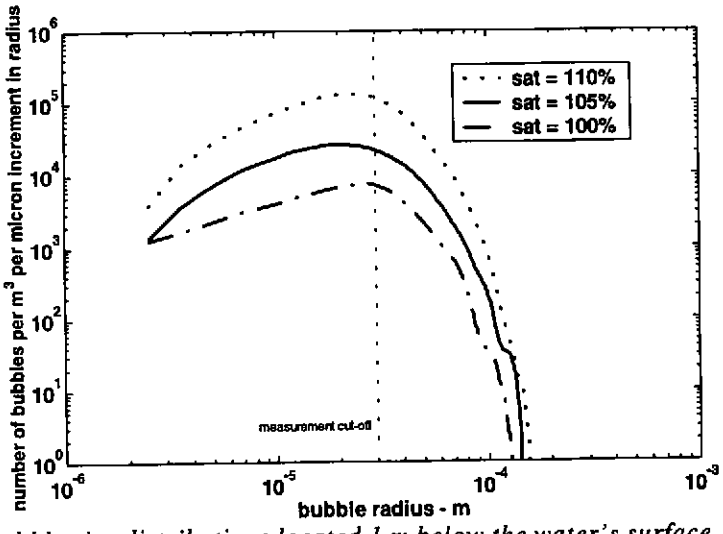

Figure 6. Modeled bubble size distributions located 1 m below the water's surface, 60 m offshore, for three different gas saturation levels. The turbulent diffusivity was fixed at 10^{-2} m^2s^{-1} for the three model runs.

bubble sizes. The effect at the larger bubble sizes results from the rising of the bubbles being retarded by the turbulence, where the 'larger' bubbles could be defined using a criterion based on their rise velocity: $w_b > u'$, where $u' \sim \frac{K}{l}$. At the smaller bubble sizes, when $w_b << u'$, the bubbles are passive to the flow and their numbers are controlled by gas dissolution and their loss due to flux across the free surface. Unlike the boundary conditions in the open ocean where bubbles are free to mix to depth, the bubbles in the surf zone are constrained by the shallow bottom. As a result, the effect of the increased turbulence levels is to bring the bubbles in contact with the surface boundary at a higher rate. For example, since the rise velocity of a 10μm bubble is expected to be 0.02 cm/s, it requires O(10^3) seconds to rise O(1) m before it is lost at the surface. In comparison, a turbulent diffusivity of O(10^{-2}) m^2s^{-1} implies a time scale of O(10^2) seconds to raise a 10 μm bubble to the surface.

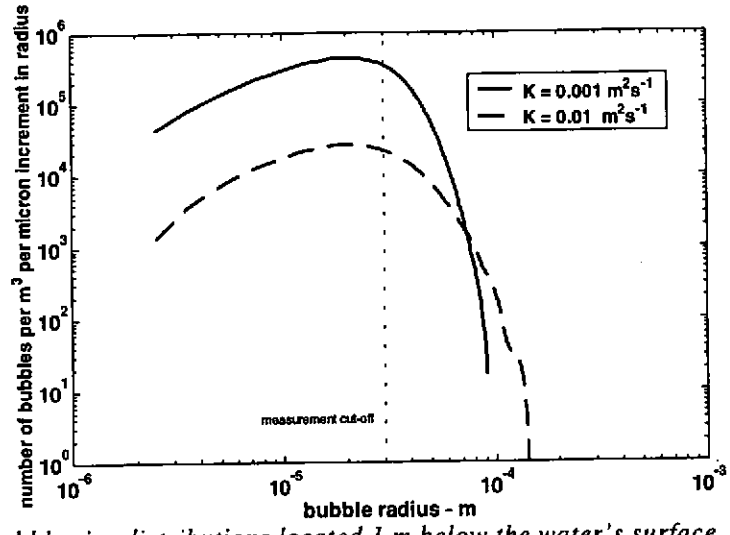

Figure 7. Modeled bubble size distributions located 1 m below the water's surface, 60 m offshore, for two different turbulent diffusivities. Dissolved gas saturation levels were fixed at 105%.

While the model adequately predicts features observed in the measured bubble sizes, the model appears to deviate from the measurements for the larger bubbles. Specifically, the model appears to underestimates the number density of the larger bubbles unless unreasonable estimates of turbulence or gas saturation levels are used. However, it is feasible that either the bubble rise speed or gas dissolution rates characterized in the model differ from what is occurring in the surf zone. In fact, the two processes may not be mutually exclusive of each other. There is evidence for this in the work of Johnson and Wangersky [16], who showed in laboratory experiments that bubbles with radii smaller than 200 μm could be stabilized by the presence of small quartz particles that adhered to the surface of the bubble. While they did not measure rise times of these stabilized bubbles, it is also

reasonable to believe that the particles may also alter the buoyancy of the bubble. Given that the rip currents have both high bubble concentrations and sediment loads, it is likely that the bubbles are partially stabilized by the particles (or surface organic compounds that are common to coastal waters) by the time they have reached distances offshore the surf-line. Clearly the effects of bubble stabilization and reduced rise times of bubbles needs to be explored more closely.

4. Conclusion

Through the use of acoustic techniques, measurements of bubble size distributions transported offshore the surf zone by rip currents have been conducted. To aid in the analysis of the data, a simple model of bubble lifetimes and transport in a rip current was developed and is found to reproduce general features of the measured bubble size distributions. While the model is simplistic in formulation, it incorporates the important physical processes which govern the lifetimes of bubble size distributions and provides a rational framework for the analysis of field measurements of bubbles. The model also provides spatial information regarding the bubble size distributions within the surf zone which can be exploited for modelling sound or optical propagation, source terms for marine aerosol generation, or bubble mediated atmospheric gas exchange. Through this combined modelling and measurement effort, guidance is also provided for continued research in this complex field.

Acknowledgements

We wish to acknowledge the support of this work by ONR Acoustics funding of the Scripps Pier Experiment and Terrill's support through the ONR Young Investigator Award. G. Lada is supported through an ONR AASERT fellowship.

References

[1] Commander KW and McDonald RJ. Finite element solution of the inverse problem in bubble swarm acoustics. *J. Acoust. Soc. Amer.* 1991; **89:** 592-597.

[2] Terrill EJ and Melville WK. A broadband acoustic technique for measuring bubble size distributions: laboratory and shallow water measurements. *J. Atmos. Ocean. Tech.* 2000; **17**: 220-239.

[3] Smith JA and Largier JL. Observations of nearshore circulation – rip currents. *J. Geoph. Res.* 1995; **100**: 10967-75.

[4] Terrill EJ, Stramksi D, and Melville WK. Bubble entrainment by breaking waves and their influence on optical scattering in the upper ocean. Submitted to *J. Geophys. Res.* 2000

[5] Phelps AD, Ramble DG and Leighton TG. The use of a combination frequency technique to measure the surf zone bubble population. *J. Acoust. Soc. Amer.* 1999; **101**: 1981-1989.

[6] Deane GB and Stokes MD. Air entrainment processes and bubble size distributions in the surfzone. *J. Phys. Ocean.* 1999; **29:** 1393-1403.

[7] George R, Flick RE, and Guza RT. Observations of turbulence in the surf zone. *J. Geophys. Res.*1994; **99**: 810-810.

[8] Keeling RF. On the role of large bubbles in air-sea gas exchange and supersaturation in the ocean. *J. Mar. Res.* **51**: 237-271.

[9] Moore DW. The boundary layer on a spherical gas bubble. *J. Fluid Mech.*, 1963 **16:** 161-176.

[10] Levich, VG. Physiochemical Hydrodynamics. Prentice-Hall, Englewood Cliffs, New Jersey, 1962, 700 pp.

[11] Thorpe, SA. On the clouds of bubbles formed by breaking waves in deep water and their role in air-sea gas transfer. *Phil. Trans. Roy. Soc. Lond.* 1982; **A304:** 155-210.

[12] Thorpe SA. A model of turbulent diffusion of bubbles below the sea surface. *J. Phys. Ocean.* 1984; **14**:841-854.

[13] Garrett C, Li M, and Farmer D. The connection between bubble size spectra and energy dissipation rates in the upper ocean. *J. Phys. Ocean.* 2000; **30**: 2163-2171.

[14] Wallace DWR and Wirick CD. Large air-sea gas fluxes associated with breaking waves. *Nature.* 1992; **256**: 694-696.

[15] Phelps AD and Leighton TG. Oceanic bubble population measurements using a buoy-deployed combination frequency technique. *IEEE J. Ocean. Eng.* 1998; **23**: 400-410.

[16] Johnson BD and Wangersky PJ. Microbubbles: stabilization by monolayers of adsorbed particles. *J. Geophys. Res.*1987; **92**:14641-14647.